Eur. Phys. J. D **28**, 241–251 (2004)
DOI: 10.1140/epjd/e2003-00301-8

THE EUROPEAN PHYSICAL JOURNAL D

Electrical characterization of atmospheric pressure arc plasmas

An overview

C. Fanara[1,a] and L. Vilarinho[2,b]

[1] School of Industrial and Manufacturing Science - Cranfield University MK430AL Cranfield, UK
[2] Federal University of Uberlândia, Campus Santa Mônica, 38400-902, Uberlândia/MG, Brazil

Received 20 August 2003
Published online 2nd December 2003 –

Abstract. The properties of atmospheric pressure arcs are investigated by means of electric exploration of plasma column and anode region. For the electrostatic probe technique, where the level of collisionality distorts the characteristic curve, data interpretation is difficult because no comprehensive underlying theory exists for the non-homogeneous electric arcs used in industry. Results are presented from an extended study of Langmuir probes applied to short, point-plane arcs. A multi-wire apparatus, operating for arc currents in the range 50–200 A is described and ion current densities and temperature maps are shown. The reduction of the probe determined temperature with respect to emission spectroscopy values is discussed and the "cooling" is ascribed to ion-electron recombination within the perturbation region formed around the probe. This region is investigated by means of emission spectroscopy and the extension found agrees both with numerical estimations and fast speed camera photographs. Diamond Like Carbon (DLC) partially coated wires can address data inversion problems and the role of arc flow directionality on charge capture and preliminary observations are shown. Charge capture and anode fall structure can be investigated using a "split-anode" technique. A prototype of a modified apparatus is described and preliminary results on the collected current are given.

PACS. 52. Physics of plasmas and electric discharges – 52.80.Mg Arcs; sparks; lightning; atmospheric electricity – 52.70.-m Plasma diagnostic techniques and instrumentation

1 Introduction

Atmospheric plasmas are widely used in technological processes, from metal welding and cutting (TIG arcs) to spray technologies for the coating industry. The region of interest for the atmospheric pressure arc on a density temperature (n, T) diagram is shown in Figure 1a, the torch assembly for the TIG arc is depicted in Figure 1b. Among the techniques used for the characterisation of laboratory plasmas, emission spectroscopy is one of the most employed but it suffers from the lower temperature limit (9–10 000 K [1,2]) so that TIG arc plasma edge temperatures are not measurable. In contrast, the relatively simpler electric (Langmuir) probe [3,4] can investigate lower temperature regions.

The main goal of this work is the determination of key parameters of industrial arc plasmas, namely electrical radius, plasma potential, temperature, current density, using the electrostatic probe technique extended to partially insulated probes and by detecting the current at the anode. In addition to the traditional Langmuir probes, which deliver line-averaged signals which require Abel inversion, wires whose surface is partly coated with diamond like carbon (DLC) have been constructed. These allow examining local signals and the influence of the directionality of the arc flow. A modified version of the split-anode technique is described, which is capable to collect the current impinging on the anode electrode.

The electrostatic Langmuir Probe technique benefits from simplicity of operation, although the interpretation of the data presents difficulties under typical atmospheric pressure flowing conditions. Several classification criteria were investigated and the results believed to be applicable to the present study were summarized in [4,5]. None of the available theories is fully applicable to the given experimental conditions and particularly, the interpretation of the characteristic V-I curve is difficult. Temperature measurements performed by Gick et al. [3] made use of the ion saturation part of the V-I curve, the only available under these experimental conditions, but gave values lower by a factor two than the spectroscopic results. In this work a method similar to Gick is employed. However, because of this flow-induced cooling in the perturbation region (PR) forming around probes, an estimate of the extension of the latter was obtained by the comparison of emission spectroscopy line intensities in presence and absence of probes. Section 2 describes the probes experimental apparatus,

[a] e-mail: c.fanara@cranfield.ac.uk
[b] e-mail: vilarinho@mecanica.ufu.br

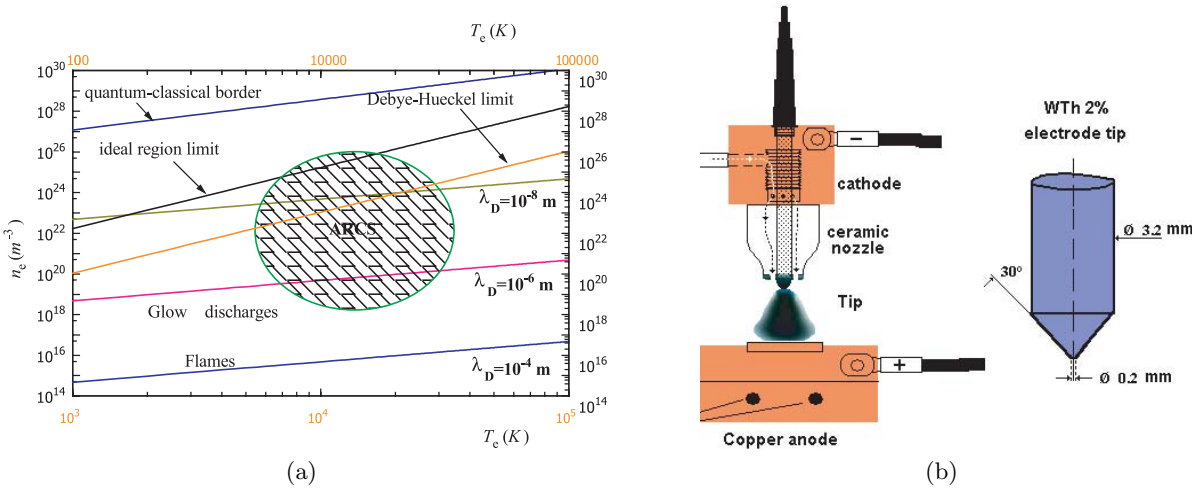

(a) (b)

Fig. 1. (a) Location of atmospheric pressure arcs on a (n,T) diagram, (b) nozzle and cathode configuration.

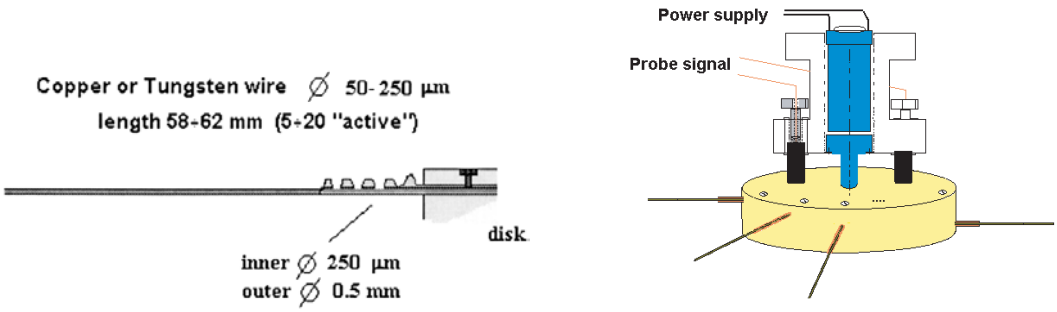

(a) (b)

Fig. 2. (a) Probe details (not to scale), (b) probes mounted on disk.

Section 3 the results obtained and Section 4 reports on conclusions and perspectives.

2 Experimental

2.1 Langmuir probes

The complete apparatus has been described elsewhere [4,5]. Here only some details on the probe system are given. A solid brass disk carries up to 12 copper probes (radius 125 μm, length 62 mm) mounted radially outwards at different heights on the disk side. These are swept at constant velocity (5.2 m/s) through an argon shielded TIG arc at atmospheric pressure. The angle between adjacent probes (30°) ensures that only one probe is inside the arc at a time. The probe length was chosen to ensure that the free end was well outside the plasma boundary, avoiding end effects, Figure 2a. On the upper disk surface a pair of carbon brushes collects the charge, Figure 2b and the signal is read as a voltage across the "high" read-out resistor $R \approx 67$ kΩ (floating conditions) or $R_L = 4$ Ω in biased conditions.

2.2 Measurement of the perturbation region (PR)

The experimental set-up is the same employed for previous probe measurements [4–6] and spectroscopic measurements [2,6]. The probe diameter has been kept at 250 μm as in the previous probe measurements and a new disk has been built to accommodate all the probes at the same height. The principle of the method is to scan the chosen (r,z) arc locations using two argon emission lines (previously employed to determine the temperature [2,6]) in absence and in presence of probes and compare the absolute intensities. Because the timing for the optical and the probe experiments is quite different, a sufficient number of probes has to be inserted at the same height within the arc. In Figure 3a the fraction of the circle interested by the probes while sweeping in the arc is shown. Figure 3b shows the five locations chosen, symmetric with respect to the arc centre, and how the total 25 scanning points (black circles) are chosen around the single location considered (empty circle).

Attempts to obtain complete maps, e.g. to take data at about 80–100 points in the (r,z) plane suffer from the problem of heat transfer to the probes at the highest currents. Therefore, the maximum time interval for the highest arc current values is kept to one hour. This is the reason why only five points were taken for each of the

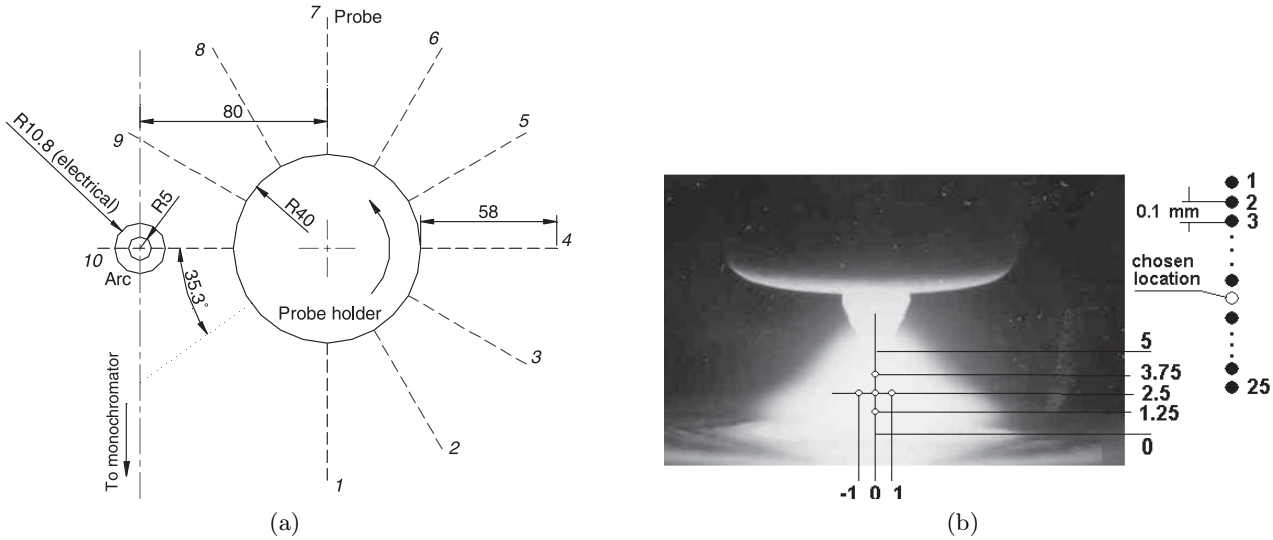

Fig. 3. (a) Set-up with 10 probes. The disk to arc centre distance is shown with a possible arc diameter [5]. The limiting angle for the shadowing to occur is also indicated ($\approx 35.3°$). (b) The five probe positions within the arc (empty circles) and choice of the corresponding 25 points to be scanned (full circles) to measure the PR extension. All distances in mm.

measurements ($z = 3.75$ (4.0 mm at 200 A), $z = 2.5$ at $r = 0$, on axis, and $r = \pm 1$ mm and $z = 1.25$ to 1.40 mm from the anode). The spectroscopy procedure consists in taking readings at 25 points, 12 per side of each of the chosen locations (12 up-stream, 12 down-stream, and the probe location). The total spectrometer read-out time is of the order of 2 seconds per point. "Blank" will always indicate emission intensities taken in absence of probes.

A fast CCD camera with digital output was used for the photographs, with a 0.5 m focal lens (Phantom V4.0, arc magnification: 6:1; 2 000 frames per second, resolution 512×256 pixels, exposure time 10 μs). The probes were mounted as in the spectroscopic experiment for the 5 mm arc, but additional photographs were taken of the 10 mm arc at the positions $z = 2.5$, 5.0, 7.5 mm from the anode with various lens apertures at arc currents of 50, 100 and 200 A.

2.3 Anode detector

In earlier attempts to investigate the arc anode region by means of the "split anode" technique [7,8], an arc travelled across the interface of two conducting blocks, insulated from each other by air or mica. The technique suffered from the need of a double Abel inversion to reconstruct the local information originating from a variable anode surface area. In the present approach, a modified version has been constructed (Fig. 4). The split anode was made of two water-cooled copper blocks separated by a sandwiched copper strip (Goodfellow 120 length mm, height 20 mm, thickness 50 μm) insulated with two ®Kapton foils (thickness 25 μm).

The current signal is read out of a 50 μm insulated copper strip clamped between the two anode blocks (common). This set-up reduces the geometry of the problem from two to one dimension.

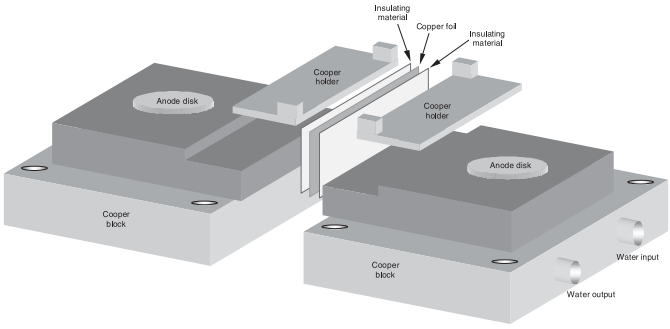

Fig. 4. The modified split anode.

3 Results and discussion

3.1 Langmuir probes

A typical set of peaks is shown in Figure 5 for biased conditions. The highest signal amplitudes correspond to the probes that are the furthest from the anode surface (the anode is taken as reference for the voltage scale).

Once Abel inverted, the signals are used to construct the characteristic curves (VI). The VI curve method can be used to determine electron temperatures, charged particle density and plasma potential. Figure 6 shows the ion portion (to the left of each graph) and the electron retarding region (steeper part) of the curves obtained by varying the bias (note that the curve is folded with respect to "textbook VI curve" [9]).

These are the only regions obtainable in the column of TIG arcs. Due to the much higher electron mobility, it is not possible to obtain the electron saturation region within these experimental limits. It can be observed that clear ion saturation occurs at "low" arc currents (Fig. 4a, 50 A) the more so the lower the probe height within

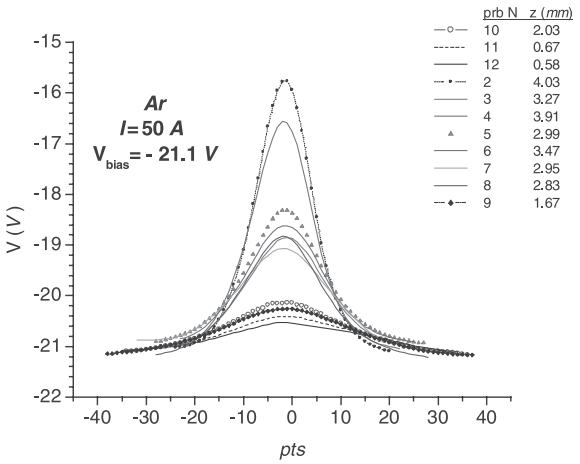

Fig. 5. Peak widths for all probes under specific bias voltage −21.1 V, close to ion saturation.

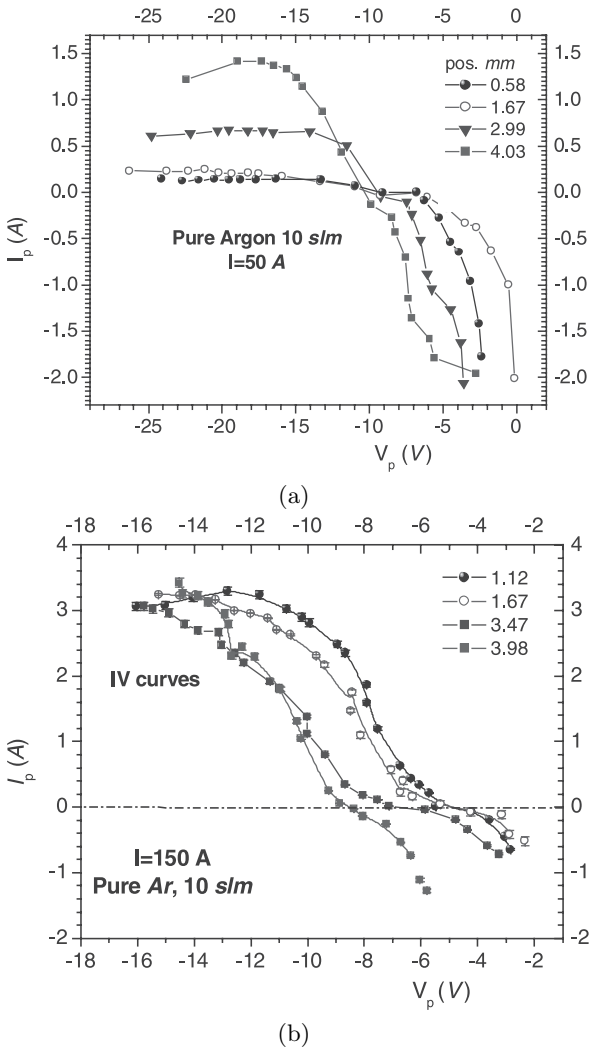

Fig. 6. Example of characteristic curves obtained from probes in TIG arc. The ion saturation part is shown but the steep region is only partial. (a) 50 A, (b) 150 A.

the arc. At higher arc currents ion saturation is less evident (Fig. 6b, 150 A). The ion saturation part can be used to infer the temperature assuming either a Continuum plus free-fall model [10,11] or a ion random flux towards the thin sheath [3,4]. The construction of a current-temperature relationship [3] using data by Olsen [12] permits to obtain the temperature. However, the latter is significantly lower than the values obtained from emission spectroscopy [6] in both the collection models considered, see Figure 7. The (steady-plasma) Continuum plus Free-Fall model provides somewhat higher values, although recent studies [5] demonstrated that the random model is the most appropriate for the system under study.

The temperature depression ("cooling"), due to relative arc probe motion has been ascribed to electron-ion recombination within the perturbation region forming around the probe [5]. It should be mentioned that the latter fully embeds the thin electrical sheath so that the temperature refers to the PR and not to the bulk of the plasma.

An axial plasma potential is obtainable from probe voltage measurements performed in floating conditions in the hypothesis of constant "contact" potential along the arc height and negligible radial field component (Fig. 8). Because this assumption is questionable, as an alternative, the plasma potential can be obtained from the probe-determined temperature. Corrections for the flow induced cooling permit comparisons with the literature. For low arc current (I = 50 A) the corrections are detrimental with respect to the data in the literature. In contrast, at higher arc currents, the correction leads to substantial agreement with the computed values by Sansonnes and Lowke [13]. In this case it is noteworthy that the forecast of a voltage inversion in the arc column, i.e. far from the electrode sheaths, is reproduced experimentally.

A *floating arc radius* can be obtained by taking the half width of the peaks obtained in floating conditions. Under these conditions, the current collected by the probe is practically zero, i.e. no substantial charge conduction can be expected at these distances from the arc axis. In contrast, the *current carrying radius* can be defined as the half width of the ion current density signal at ion saturation. This is the region where the conduction takes place. Beyond this radial distance, the charge collected is close to zero, which justifies the nomenclature of the region as "electrical halo". For example, Figure 9 shows the two radii at 50 and 200 A. Both radii increase with total arc current. The number of collected ions (measured current) has been compared with the number of ions present at the same location and temperature based on the hypothesis of LTE.

It was shown that the collected absolute number of particles (within the probe elemental volume) is up to two orders of magnitude lower than the number of particles contained within the same volume in LTE conditions [5]. Bearing in mind the degree of uncertainty in both the directly measured and in the temperature-computed number of particles, still it appears that the hypothesis of a probe collecting the correct number of charges

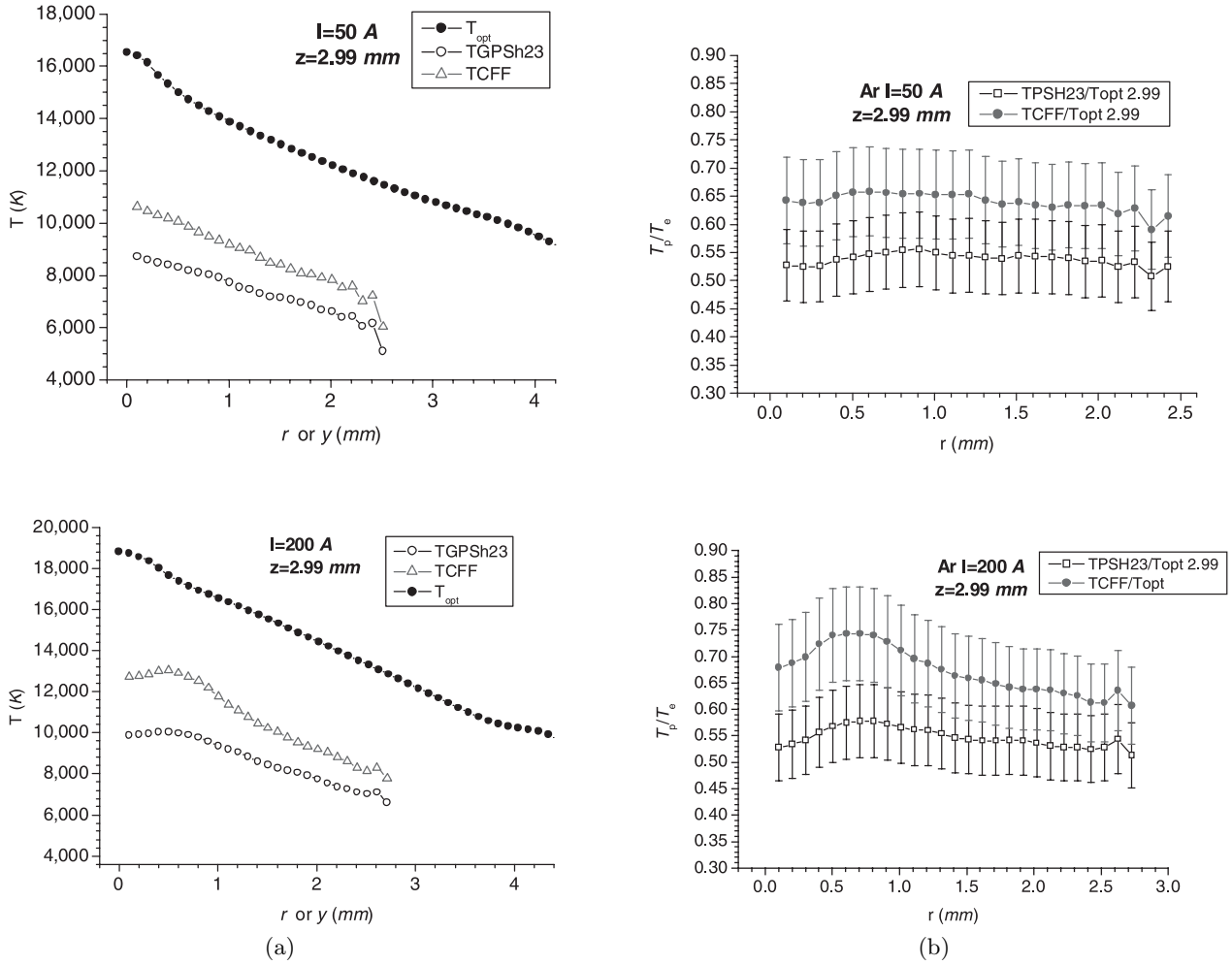

Fig. 7. Comparison between probe and optical temperatures at $z = 2.99$ mm at $I = 50$ and 200 A. (a) Optical emission temperature (full circles), continuum plus free fall theory (CFF, triangles) and random (TGPSh23, [3]) with pre-sheath and partial collecting surface (empty circles). (b) Ratios of probe determined to optical emission spectroscopy.

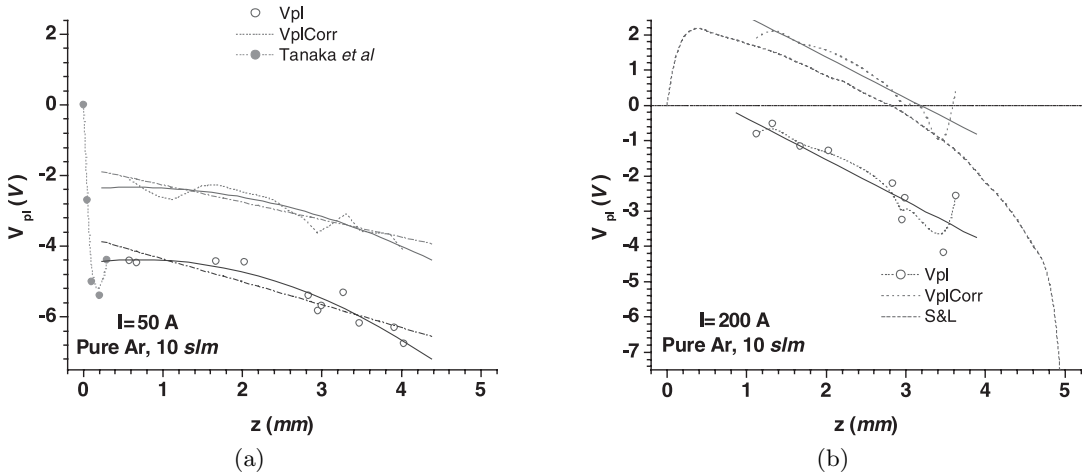

Fig. 8. Axial plasma potential for $I = 50$ and 200 A. (a) For 50 A (uncorrected data empty circles, corrected values dotted line) comparison is made with measured values of Tanaka et al. [14] obtained in the anode region (full circles). (b) The 200 A case (same symbols) is compared with the model of Sansonnes and Lowke (S&L, [13]).

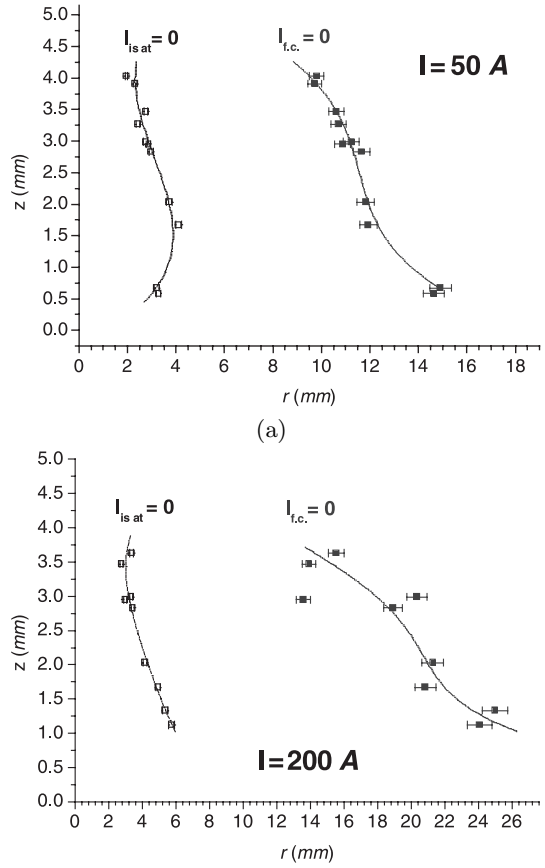

Fig. 9. Edges (where $I = 0$) of the inverted peaks as a function of position, e.g. "internal" or current carrying region and external or "halo" electrical radius. (a) $I_{arc} = 50$ A, (b) $I_{arc} = 200$ A. Legend: I_{sat}, ion current in biased conditions at saturation; $I_{f.c.}$, current in floating conditions.

locally available is not unrealistic. This implies that the ion current density at ion saturation *is representative* of the plasma ion current density and as a consequence, the inner electrical radius could truly represent the extent of the current carrying region. The shape of the radial distribution confirms this indication. By collecting all the (j, r) maps from the Abel inverted currents, the ion current density can be represented by the two-dimensional maps of Figure 10, for arc currents from 50 to 200 A.

These figures show that increasing the arc current from 50 to 100 A, the inner (most luminous) region expands towards the anode and from 150 A upwards, is distributed more uniformly along the arc length.

3.2 Perturbation region

For consistency check, the curves obtained with the two emission lines (696.54 and 706.72 nm) were compared. Because these correspond to different excitation states of atomic argon, they differ somewhat, but provide electron temperatures which agree well within the experimental error [2,6].

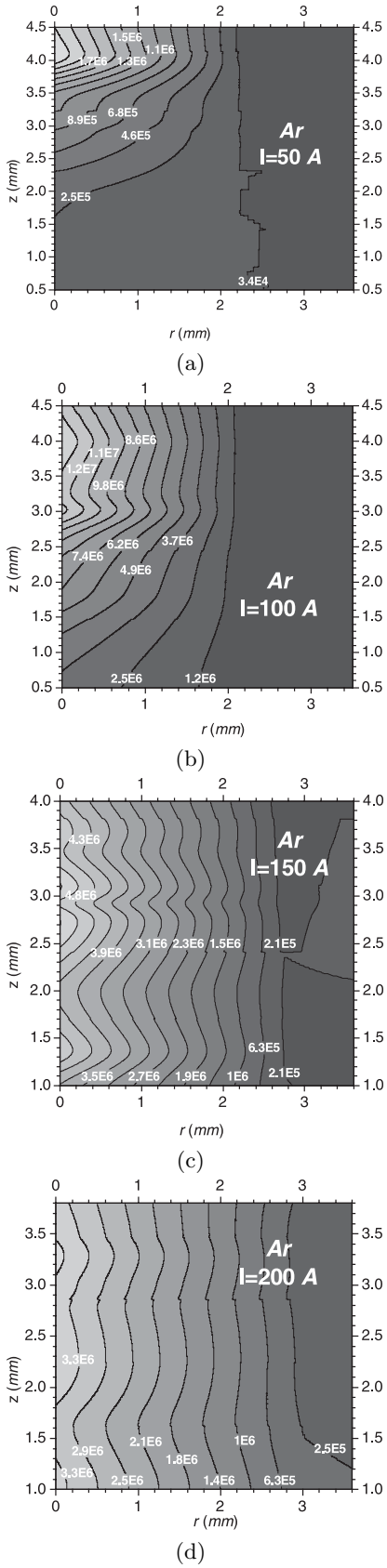

Fig. 10. Two-dimensional maps for the ion saturation current density (A/m^2). Arc currents: from above, 50, 100, 150 and 200 A.

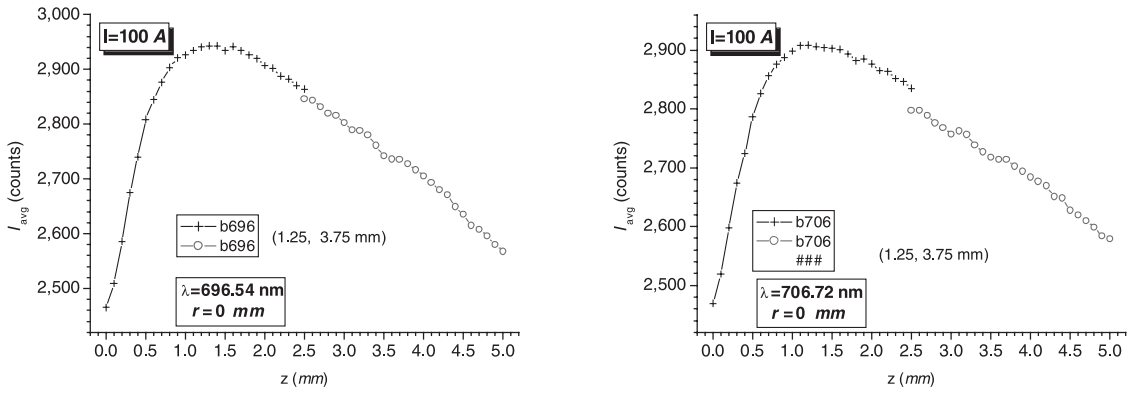

(a) (b)

Fig. 11. Blank consistency for two different lines at $I = 100$ A. (a) $\lambda = 696.54$ nm, (b) $\lambda = 706.72$ nm. The branches indicated by the different symbols correspond to sets of data (full circles of Fig. 3b) taken for two different points (empty circles of Fig. 3b).

The variation of the integrated intensity with the arc height, non monotonic, is consistent with the expected behaviour of the emission coefficient as a function of height (Fig. 4, [2]). In fact, the arc section decreases as the arc height increases, causing a lowering of the integrated intensity. In contrast, the intensity increases as the temperature rises with the arc height. These two effects can be appreciated observing the number of counts for the "blanks" between the different axial regions, which match in the complete curves, 0 to 5 mm in Figure 11. Note that in all the curves showing the emission intensity as a function of height, the flow is oriented from high to low z (e.g. right to left, cathode to anode).

The comparison between the curves obtained with and without probes as a function of the height z gives an appreciation of the PR extension. For quantitative purposes, the averages of the curves obtained with probes are compared with the averages of the "blank curves" obtained with two argon lines acquired simultaneously (696.54 and 706.72 nm). These comparisons are shown in Figure 12 where the estimate of the PR thickness is indicated for each of the arc currents. The spectroscopic measurements agree with computed data [15].

The difference of the counts is lower at higher probe position, even if the number of counts is lower in the blanks. This suggests that the probe "shadowing effect" is less marked at higher axial positions. As noted earlier, the greater the height, the smaller the arc section. Thus the (line) integrated intensity is lower for both signals and blanks. If this reduction, due to the smaller section, is the same with and without probes, the reduced contribution of the signals with probe would dominate. However, this assumption implies undisturbed arc, thus to avoid circular argument, a series of photographs was taken to check for discernible variations of the arc diameter at the probe chosen height. Figure 13, referring to the 50 A case, shows a reduction of the section by ∼14% (to the original photographs a numerical algorithm was applied in order to appreciate the contrast of different arc regions [16]). Thus the line-integrated intensity is reduced by the combined effect of probe shadowing under "undisturbed conditions" and by the arc radius reduction. It is difficult to discriminate the two effects. For the 200 A case shown in Figure 14, the reduction of the arc section due to probe presence is much less marked. Also from Figure 12, it can be observed that the width of the perturbation region is always lower as the arc height increases. This is expected because in the region closer to the cathode the flow velocity is higher and in the idealized "free-stream" conditions one would expect a thinner boundary layer. In contrast, it is not possible to conclude on the extension of the PR as a function of the arc current (the data points are scattered at 1.25 mm, perhaps increasing at 3.75 mm). Also, these graphs show that with the exception of the $I = 50$ A case, the up-stream part of the PR is less extended. The PR thickness obtained is approximate because of the probe positioning and alignment, with a resulting error on the axial coordinate (z), estimated in 200 μm on each point, close to one probe diameter (250 μm).

Should the conditions allow for the existence of a "free stream", the PR could be identified with the boundary layer and an estimate of the velocity at the edge could be attempted. However, the extension of this PR is of an order of magnitude comparable with the overall length of the plasma arc in the 5 mm point-plane geometry. The latter circumstance makes the mentioned identification unjustified.

In fact, the complete sequence of photographs at different currents, especially of the arc core, where velocity and temperature gradients are steeper, and of the envelopes, indicates that the perturbation takes place beyond the expected "Boundary layer" extension allowed by a free-stream theory, estimated previously in a fraction of a millimetre [5].

With this limitation in mind, a visual inspection of Figure 14 (200 A, 5 mm) suggests a PR extension which amounts to 30 to 35% of the arc length; the up-stream extension is 1 to 2% of the arc length and the remaining of the PR is due to the down-stream portion of the PR. The asymmetry tends to disappear for lower probe positions

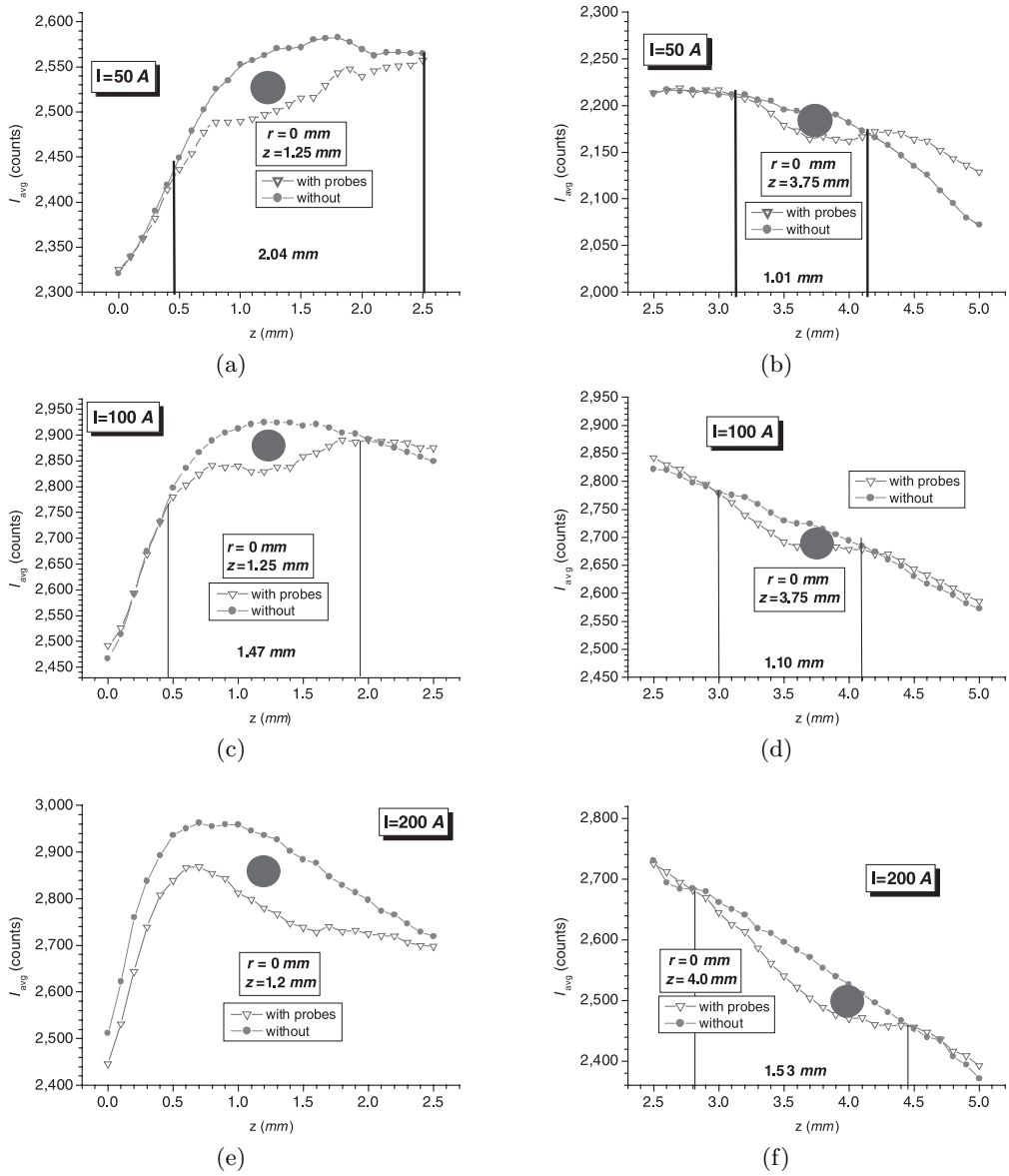

Fig. 12. Signal and blanks averaged over the two different wavelengths at the positions $r = 0$, $z = 1.25$ and $r = 0$, $z = 3.75$ mm. From above 50 A (a, b), 100 A (c, d) and 200 A (e, f) the latter is $z = 1.2$ and 4.0 mm instead of 1.25 and 3.75 mm.

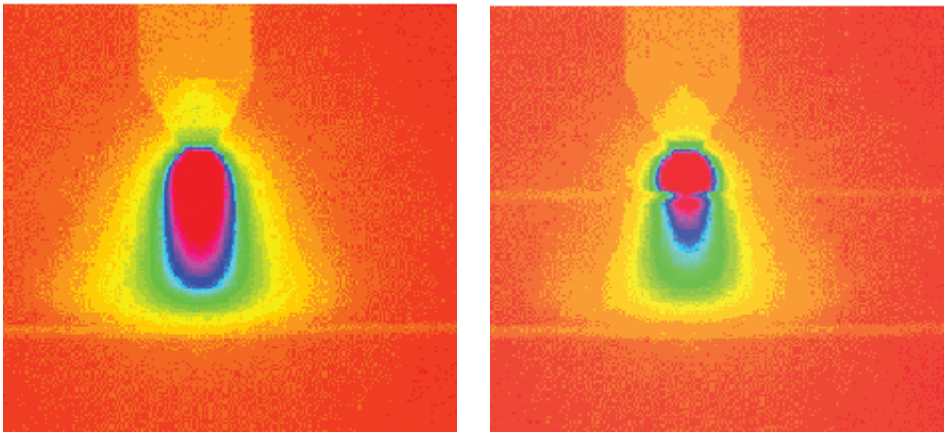

(a) (b)

Fig. 13. $I = 50$ A. Example of probe perturbation obtained from high-speed camera films (aperture $f8$). Arc length 5 mm. (a) Without probe, (b) with probe at $z = 3.75$ mm.

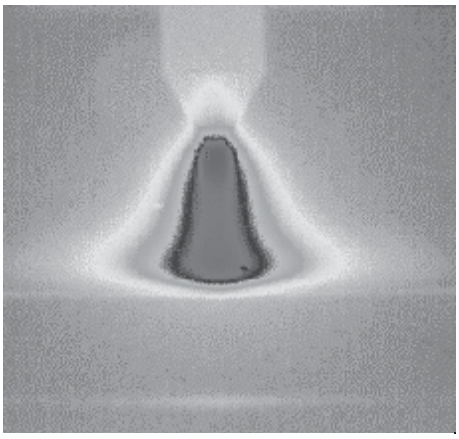

(a)

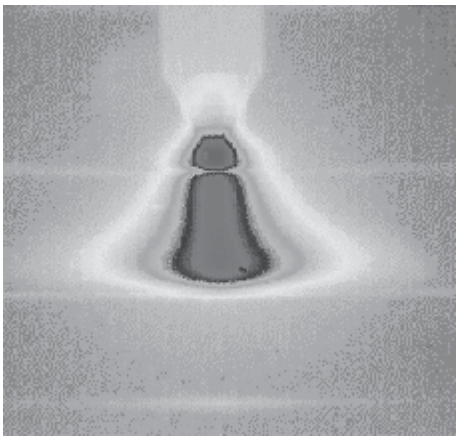

(b)

Fig. 14. I = 200 A. Example of probe perturbation obtained from high-speed camera films (aperture $f22$). Arc length 5 mm. (a) Without probe, (b) with probe at $z = 3.75$ mm.

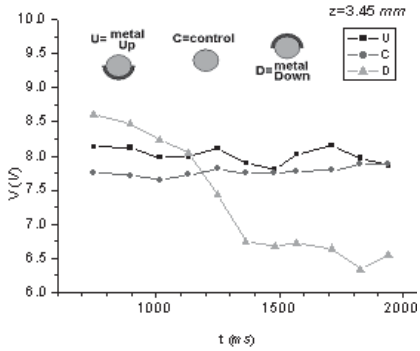

(a)

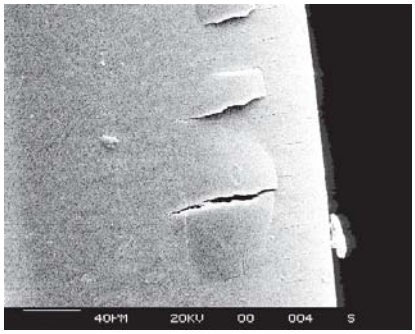

(b)

Fig. 15. (a) Current signals (left axis) and corresponding voltages (right axis) from DLC coated copper probes (U = metal up, C = control, D = metal down, see text). (b) Delamination due to wire-coating thermal mismatch (Coating thickness, 5 μm).

(below mid-arc, towards the anode). This is in agreement with the spectroscopic measurements (cf. Fig. 12). Therefore, despite the semi-quantitative nature of this particular analysis, two conclusions are possible: (1) there is clear asymmetry between the up- and down-stream probe regions at high arc length and (2) the PR extension increases with the arc length. In the first instance, there is some experimental evidence [17] of orientation dependent charge capture on cylindrical probes, with "active" surface variable from half to two-thirds of the up-stream probe surface [17,18]. If this is correct, the fact that the PR is *less extended up-stream* of the probe indicates that the relevant plasma parameters could be obtained from the up-stream surface within the limitation of a "small" disturbance. Therefore, *for this purpose*, the found asymmetry between up- and down-stream regions could be ignored.

3.3 DLC coated probes

So far, tests were performed with probes half-coated along the axial direction. The *electron* current signals shown in Figure 15a were obtained in conditions close to floating at $I = 50$ A using three probes placed at 2 mm from the anode: *metal up*, *control* (uncoated) and *metal down*.

In the initial stages (about 300 ms), possibly due to coating disruption, the contribution from "down" probe

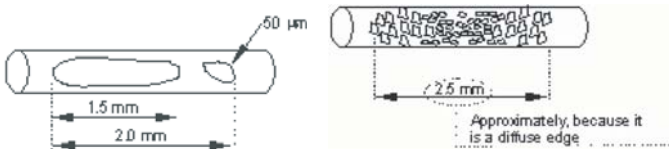

(a) (b)

Fig. 16. Schematics of coating damage upon immersion in arc at 50 A, (a) metal-up probe at $z = 2.0$ mm, (b) metal-down at $z = 2.0$ mm.

dominates but after decay, it remains always lower than the contribution of probes with conducting surfaces facing the cathode (metal up). Despite the use of controlled inert (Ar) atmosphere, DLC delamination occurs due to the difference in the thermal expansion coefficients of substrate (Cu initially, but later also W) and coating (DLC, 5 μm), cf. Figure 15b. A systematic study of the delamination was performed and some differences in the up- and down-stream exposed surface were observed as indicated in Figure 16.

To overcome the problem, a graded (WC and DLC) was developed at Cranfield [19] and new spot-uncoated probes are under testing. The main advantage of the latter is that it delivers local values of the current avoiding the Abel inversion procedure.

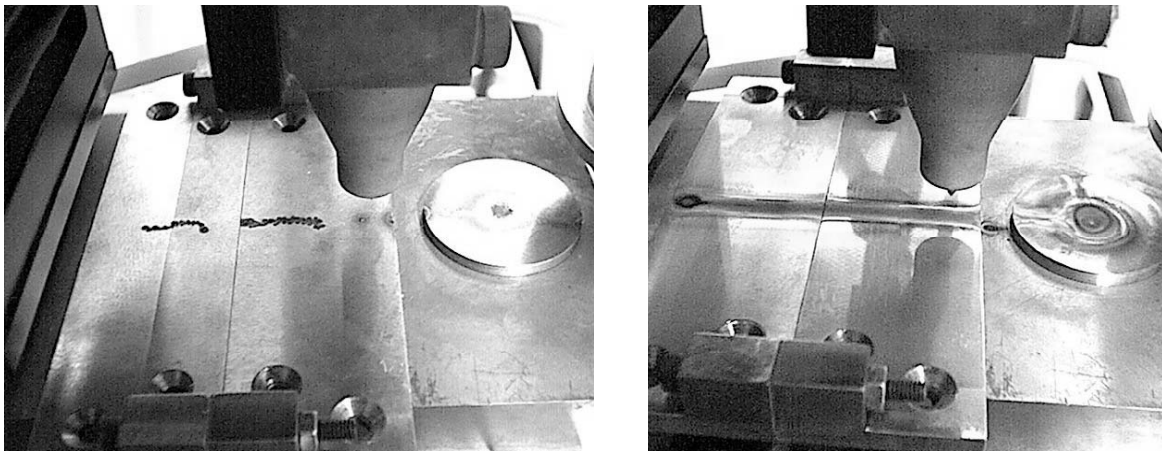

(a) (b)

Fig. 17. Arc path trace on the two copper blocks, $I = 50$ A. (a) Travel speed = 10 mm/s. (b) Travel speed 60 mm/s. The interface and the anode disk where the arc is struck before — and after the split anode motion — are also shown.

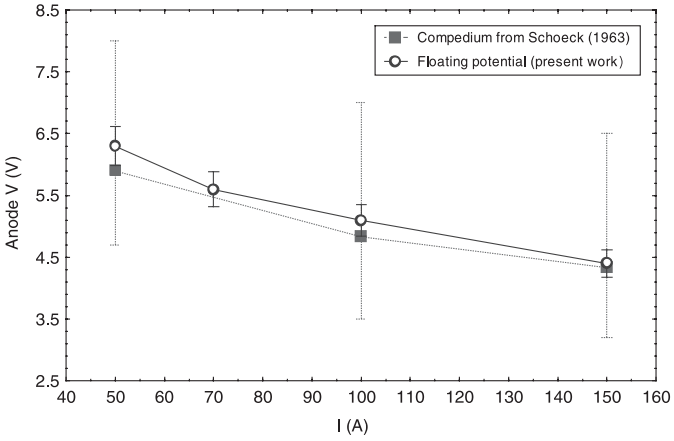

Fig. 18. Comparison of voltage falls reported by [8] (full squares) and this work (empty circles) as a function of arc current.

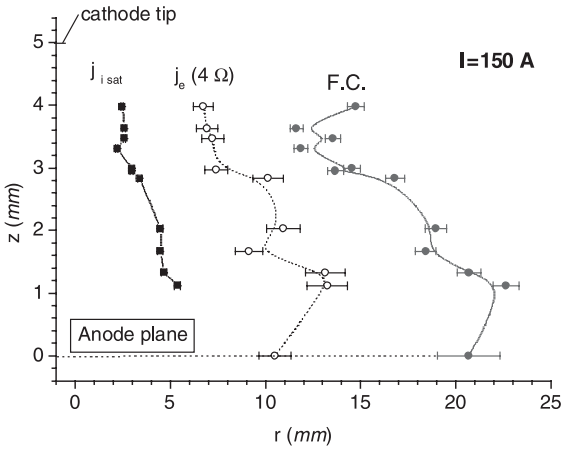

Fig. 19. Arc electrical radii: from ion saturation of V-I curves (probes in arc column only, full squares), electron current density under zero bias (probes in arc and anode detector, empty circles) and from floating conditions (probes in arc and anode detector, full circles).

3.4 Anode detector

In order to verify reproducibility and stability and uniformity of arc motion, the split anode set-up was moved back and forth in two subsequent passages of the arc across the interface, providing two experimental signals. Both the calculations and the signal gathered during the travel, rule out any noticeable asymmetry of the arc. Stability and reproducibility of the signals were achieved by the choice of a travel speed of 60 mm/s. In Figure 17 the traces of the arc path are shown for (a) 10 and (b) 60 mm/s.

Moreover, the signals obtained for different arc currents show a monotonic decrease of the voltage similar to probe floating in the arc column. Figure 18 shows a comparison between the voltage values obtained in floating conditions and the values of Schoeck [8].

Also, agreement with data from probes in the column of the arc [20] exist, indicating that an arc constriction takes places at the electrodes as expected [21] and visually observed. This is shown in Figure 19 where the radius obtained from the electron current density (empty circles) and floating conditions (full circles) is shown in conditions which are the closest to "plasma potential" (zero bias).

Measurements in biased conditions are currently under way at Cranfield.

4 Conclusions

Atmospheric pressure electric (TIG) arcs, inhomogeneous both radially and axially (ionization, temperature) can be investigated by means of Langmuir probes, but the characteristic curve is incomplete and only the ion saturation part can be constructed. The use of direct methods allows reconstructing the temperatures. However, these determinations are from 50 to 60% of the values obtained by emission spectroscopy. The major contribution to this

reduction is boundary layer cooling due to electron-ion recombination. The thickness of this layer, more exactly indicated as "perturbation region" has been obtained experimentally and agrees with previous numerical predictions and qualitatively with fast speed camera photograph. Also, its up-stream extension is less than in the down-stream region of the probe.

Axial values of the electric field can be obtained but the hypothesis that the probe to plasma contact potential (floating potential) does not vary appreciably with axial distance is unjustified. Values of the plasma potential obtained from the temperatures corrected for cooling, partly agree with the literature. The width of signals obtained in floating and biased conditions reveals a halo (no substantial current conduction) and a narrower current carrying region respectively. The use of coated probes has only been partially successful up to now due to coating delamination, and preliminary indications of directional charge capture need confirmation. The modified split-anode detector showed voltages value in agreement with previous data and it is a promising tool for the mapping of the current density at the anode.

EPSRC funded projects, grant Nr. GR/L8 2281, and Nr. GR/NB2648/01

References

1. M.F. Thornton, Ph.D. thesis, Cranfield University, 1993
2. L.O. Vilarinho, *Optical emission spectroscopy*, Internal Report Cranfield University, Cranfield, 2002
3. A.E.F. Gick, M.B.C. Quigley, P.H. Richards, J. Phys. D: Appl. Phys. **6**, 1941 (1973)
4. C. Fanara, I.M. Richardson, J. Phys. D: Appl. Phys. **34**, 2715 (2001)
5. C. Fanara, Ph.D. thesis, Cranfield University, 2003
6. C. Fanara, L.O. Vilarinho, Optical and electrical measurements in atmospheric pressure arcs: a comparison in *Annual Gaseous Electronics Conference* (GEC02), Minneapolis, MN, USA 2002
7. O. Nestor, J. Appl. Phys. **33**(5), 1638 (1962)
8. P.A. Schoeck, An investigation of the anode energy balance of high intensity arcs in argon in *Modern Developments in Heat Transfer*, edited by W. Ibele (Academic Press, 1963)
9. J.B. Cobine, *Gaseous conductors* (Dover, New York, 1958)
10. J.D. Swift, S. Schwar, *Electrical probes for plasma diagnostics* (Iliffe, London, 1970)
11. P.M. Chung, L. Talbot, K.J. Touryan, *Electric probes in stationary and flowing plasmas: theory and application* (Springer, New York, 1975)
12. H.N. Olsen, Phys. Fluids **2**(6), 614 (1959)
13. L. Sansonnes, J. Haidar, J.J. Lowke, J. Phys. D: Appl. Phys. **33**, 148 (2000)
14. M. Tanaka, M. Ushio, J. Phys. D: Appl. Phys. **32**, 906 (1999)
15. M.T.C. Fang, JinLing Zhang, J.D. Yan, Can Langmuir Probe be used for the diagnostics of atmospheric thermal plasmas with gas motion? Paper ISPC-343 in *16th International Symposium on Plasma Chemistry*, Taormina (Italy), 22-27 June 2003
16. L.O. Vilarinho, *Assessment of shielding gases by means of numerical and experimental techniques*, Qualification exam, UFU, Brazil, 2001
17. H. Tsuij, H. Toshisuke, AIAA J. **11**(1), 100 (1973)
18. M.S. Benilov, J. Appl. Phys. **70**(11), 6726 (1991)
19. Courtesy of Prof. J. Nicholls, 2003
20. C. Fanara, Electrical characterization of atmospheric pressure arc plasmas in *EMRS Symposium A-TPP7 (Thermal Plasma Processes)*, poster presentation, Ref. Nr. 0356A, Strasbourg, France, 18-21 June 2002 to be published in High Temperature Journal, edited by Prof. J. Amouroux, P. Fauchais
21. J.F. Lancaster, *The Physics of Welding* (Pergamon Press, Oxford, 1983)